Organic & Biomolecular Chemistry

Accepted Manuscript

This article can be cited before page numbers have been issued, to do this please use: M. Macias-Contreras, K. Daykin, T. Simmons, J. Allen, Z. Hooper, M. Davidson and L. Zhu, *Org. Biomol. Chem.*, 2017, DOI: 10.1039/C7OB02235B.

ROYAL SOCIETY OF CHEMISTRY

rsc.li/obc

View Article Online
DOI: 10.1039/C7OB02235B

Progressive Structural Modification to a Zinc-Actuated Photoinduced Electron Transfer (PeT) Switch in the Context of Intracellular Zinc Imaging

Miguel Macias-Contreras,[†,¶] Kirsten L. Daykin,[†,¶] J. Tyler Simmons,[†] John R. Allen,[‡] Zachary S. Hooper,[†] Michael W. Davidson,[‡,§] and Lei Zhu[†]*

[†]Department of Chemistry and Biochemistry, Florida State University, 95 Chieftan Way, Tallahassee, Florida 32306-4390, United States

[‡]National High Magnetic Field Laboratory and Department of Biological Science, Florida State University, 1800 East Paul Dirac Drive, Tallahassee, Florida 32310, United States

[¶]These two authors contributed equally.

[§]Deceased on December 24, 2015

KEYWORDS. Zinc sensor, photoinduced electron transfer, BODIPY, coumarin

ABSTRACT. Photoinduced electron transfer (PeT)-type fluorescent molecular switches are often applied in ion-selective sensors. Zinc-targeting sensors that contain an anilino-based electron donor (aka, the PeT 'switch') have multiple advantages over those with an aliphatic amino switch. In addition to the lower pK_a value of an aniline than that of a comparably

View Article Online
DOI: 10.1039/C7OB02235B

substituted aliphatic amine, which reduces the interference of pH on the spectral properties of the attached fluorophore, the oxidation potentials of anilino groups are lower than those of aliphatic amino counterparts, which make them better electron donors in PeT. The effectiveness of anilino as a PeT switch is evaluated in a series of zinc-sensitive sensors that contain different fluorophores, zinc-binding ligands, and alkyl linkers between ligand and fluorophore. The abilities of these compounds to distinguish high and low intracellular zinc concentrations in living cells are demonstrated.

Introduction

Despite being considered a trace metal ion, the total cellular concentrations of zinc are in the range of hundreds of micromolars,[1, 2] most of which are tightly associated with proteins. The so-called 'free zinc', which garners tremendous attention in zinc biology due to its functions in signalling processes, refers to zinc ions that are not tightly bound to proteins and therefore kinetically mobile for recruitment by proteins and/or for exchange between different targets.[3, 4] 'Free' zinc is actually coordinated to a diverse set of ligands as encountered within the complex and heterogenous cellular environment that are far from thoroughly characterized.[5] It is generally accepted that 'free' zinc concentrations in a cellular context swing between picomolar to hundreds of micromolar on spatial and temporal coordinates,[6-9] the acquisition of such data is of interest to researchers in the area of zinc cell biology.

Fluorescence microscopy is a powerful technique that allows not only the visualization of subcellular structures but also the intracellular distribution and trafficking of substances of interest with the help of target-selective fluorescent sensors.[10, 11] The targets can be macromolecules, small molecular metabolites, or ions, which include 'free' zinc ions.[11] The

View Article Online
DOI: 10.1039/C7OB02235B

sensors can be constructed from fluorescent small molecules or genetically encoded fluorescent proteins.[12-18]

A molecular fluorescent sensor contains two domains: a fluorophore that is responsible for absorbing and emitting photons, and a receptor (or ligand) that selectively interacts with the target, such as zinc, in the presence of a plethora of potentially interfering species. The receptor needs also to act as a trigger to alter either the color (wavelength) or brightness (extinction coefficient at the excitation wavelength and/or fluorescence quantum yield) of the fluorophore through various signal transduction mechanisms.[19, 20] These mechanisms were proposed based on sound theories long ago, which have since led to the successful constructions of effective small molecular sensors. For many other sensors that were developed empirically, the working mechanism of which were later explained by these ideas. However, challenges often emerge especially when the strongest interaction with an analyte (as often measured by dissociation constant K_d) and the largest dynamic range of analyte-dependent signal (measured by emission intensity ratio of target-bound and target-free states) cannot be satisfied simultaneously, with the consideration that the use of these sensors shall not be deterred by the cost of their syntheses. Herein, we report such a case in which progressive structural modification on a sensor structure was carried out to result in zinc-selective sensors with various combinations of sensitivity and signal dynamic range.

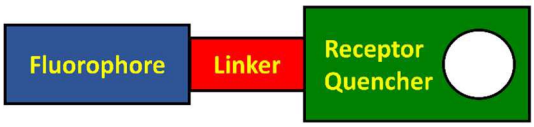

Fig. 1 A cartoon drawing of a fluorescent PeT sensor. Adapted from the work by de Silva and co-workers.[21]

View Article Online
DOI: 10.1039/C7OB02235B

Many ion-selective sensors are made based on the principle of target-actuated photoinduced electron transfer (PeT) switching, as articulated by de Silva and co-workers in the early days of fluorescent sensor research.[19] The receptor in a PeT switch acts as a fluorescence quencher, which could be inactivated via the interaction with the target. There is also a linker that covalently joins the receptor/quencher and the fluorescent reporter (Fig. 1). For the design of cation sensors with a fluorescence turn-on response, in the absence of the target, the receptor is electron-rich and therefore capable of donating an electron to the excited state of the fluorophore, thus quenching the fluorescence. Upon binding to the target cation, the electron-donating ability of the receptor is diminished, and consequently the emission intensity of the fluorophore increases.[22]

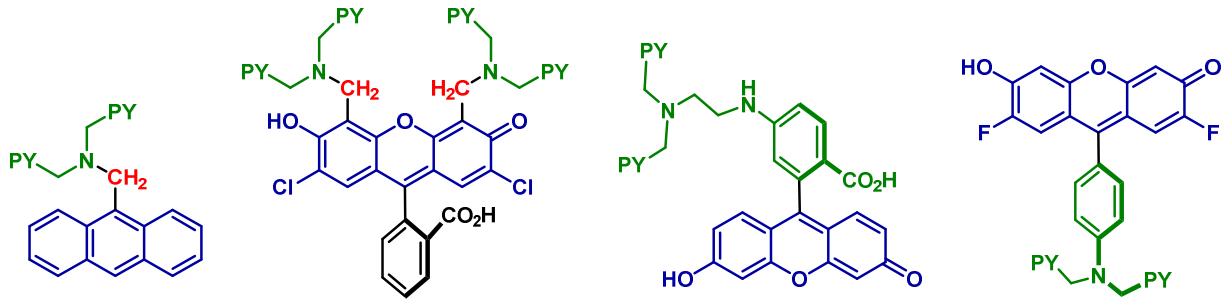

Fig. 2 Four examples of zinc-selective molecular sensors that operate via PeT-switching mechanism. Blue – fluorophore; red – linker; green – zinc receptor/electron-donating quencher. PY = 2-pyridyl; N.R. = not reported.

View Article Online
DOI: 10.1039/C7OB02235B

Four fluorescent sensors targeting zinc ions are shown in Fig. 2 to illustrate the zinc-actuated PeT switching mechanism. The colors used in the drawings match the colors in Fig. 1 that identify fluorophore (blue), linker (red), and receptor/quencher (green). Polyaza ligands that include pyridyl and amino groups are commonly employed receptors for zinc ions, such as di(2-picolyl)amino (DPA),[13, 21] which have higher affinity for zinc than for biologically abundant alkali and alkaline earth metal ions.[23]

Compound **1** (Fig. 2) was reported by de Silva and coworkers,[24] which is the product of a straightforward application of the PeT-switch strategy to construct fluorescent sensors for zinc. The DPA group is connected to the anthryl fluorophore via a methylene linker. Electron transfer from the tertiary amino group to the excited anthryl fluorophore followed by back electron transfer relaxes the excited fluorophore non-radiatively, i.e., quenches the fluorescence. This action is turned off when zinc and the amino group bond coordinatively. DPA also acts as the electron transfer quencher and zinc receptor in **ZP1** (Fig. 2),[25, 26] reported by Lippard and coworkers.

ZnAF2 (Fig. 2) is a fluorescein-containing zinc sensor developed by the Nagano group.[27, 28] Differing from **ZP1**, the electron transfer quencher moiety is a substituted anilino group. The anilino group together with the DPA moiety forms a tetradentate ligand for zinc. Lastly, **Newport Green PDX** (Fig. 2)[29] also includes an anilino nitrogen for both zinc binding and fluorescence quenching purposes.

Based on the data on **ZnAF2** and **Newport Green PDX** (Fig. 2), the anilino group is shown to be an effective electron transfer quencher[30, 31] in zinc sensor design.[32] However, the affinity value of **Newport Green PDX** (K_d = 40 μM) is lower than the aliphatic DPA-containing zinc dye **1** (K_d = 5 μM), which has the same tridentate DPA ligand. Furthermore, syntheses of zinc

View Article Online
DOI: 10.1039/C7OB02235B

sensors containing anilino groups are usually not as straightforward as aliphatic amino-containing counterparts. For example, dialkylation of anilino to produce an anilino-DPA moiety often takes days to complete.[33, 34] The underwhelming affinity to zinc and the challenges in synthesis might have hindered the use of anilino-derived ligands as receptors and quenchers in zinc sensors.

In our previous work,[35-37] it was shown that a fluorophore and an electron-rich zinc ligand can be conveniently connected via the copper-catalyzed azide-alkyne cycloaddition reaction to afford PeT-based zinc sensors. The compounds we have reported thus far contain fluorophores that are excited in the UV region, which do not work well within the technical constraints of commercial laser scanning confocal fluorescence microscopes,[10] in particular with the excitation laser sources in the visible region and the glass optic systems that strongly absorb UV. We began this study in a naive attempt to structurally modify one of our earlier UV-absorbing compounds by replacing the fluorophore with a visible light-absorbing one. Only with the subsequent structural alternations of the linker and zinc ligand components did we produce PeT-based zinc sensors that are excitable in the visible range. This work, we believe, offers a robust modular strategy to produce zinc sensors with various affinities and emission colors, without taxing synthetic efforts.

Results and Discussion

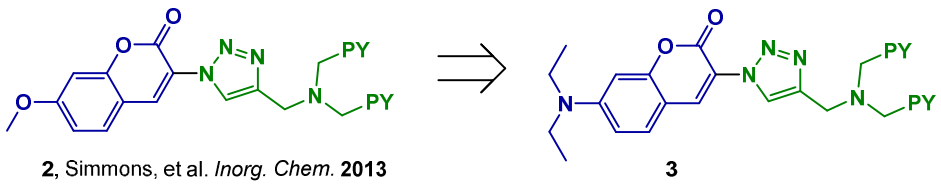

2, Simmons, et al. *Inorg. Chem.* **2013** **3**

View Article Online
DOI: 10.1039/C7OB02235B

Fig. 3 Changing the fluorophore of compound **2**[37] from 7-methoxycoumarin to 7-(*N*,*N*-diethylamino)coumarin in compound **3**.

1. From **2** to **3** – changing the fluorophore in an existing PeT-based sensor failed to retain its switching ability. Compound **2** (Fig. 3) was reported by our group to respond to the change of zinc under neutrally buffered aqueous conditions sensitively.[37] The fluorescence quantum yield of **[Zn(2)]** (shorthand of the zinc complex of **2** with 1:1 coordination stoichiometry) is 16-fold over that of **2** alone. **[Zn(2)]** has a dissociation constant (K_d) of 5.5 nM. The deficiency of compound **2**, in the context of being an agent for imaging zinc in living cells, is the lack of absorption in the visible region. That makes the technical aspects of imaging challenging, because the UV excitation light would largely be absorbed by the optical system instead of the specimen. This is a well-cited motivation to incorporate long-wavelength absorbing dyes in molecular indicators so that their spectral profiles match properly with the optical setup of commercial microscopes. In an attempt to increase the absorption cross section in the visible region based on the structure of compound **2**, specifically at 405 nm which is a laser line available to our fluorescence microscope, the UV-absorbing 7-methoxycoumarin in **2** was replaced with 7-(*N*,*N*-diethylamino)coumarin in **3** (Fig. 3), which had been reported for a different purpose.[38] 7-(*N*,*N*-diethylamino)coumarin has an extinction coefficient exceeding 2×10^4 $cm^{-1} \cdot M^{-1}$ at 405 nm. However, this structural alteration completely abrogated the fluorescence turn-on response of compound **2** to zinc that is expected from PeT-based sensors (Fig. S1).

2. Examining the thermodynamics of PeT in fluorophore-ionophore pairs. The failure in achieving zinc-switched PeT in compound **3** prompted us to examine the thermodynamic driving

View Article Online
DOI: 10.1039/C7OB02235B

forces of photoinduced electron transfer (ΔG°_{PeT}) of **3** in its zinc-free form, and other hypothetical pairings of fluorophore and electron donor. ΔG°_{PeT} can be expressed in a combination of 4 terms using the Rehm-Weller equation (eq. 1).[39]

$$\Delta G^{\circ}_{PeT} = E_{ox} - E_{red} - E_{0,0} - \frac{e^2}{d\varepsilon} \quad (1)$$

$$D^{\cdot} \rightarrow D^{\cdot +} + e \qquad E_{ox} \quad (2)$$

$$A + e \rightarrow A^{\cdot -} \qquad -E_{red} \quad (3)$$

$$A + h\nu \rightarrow A^{*} \qquad E_{0,0} \quad (4)$$

$$E(columbic) = -\frac{e^2}{d\varepsilon} \quad (5)$$

The energies associated with the formation of radical cation (eq. 2) and radical anion (eq. 3) from the neutral electron donor and acceptor are E_{ox} and $-E_{red}$, respectively. The photon energy (0-0 transition) for exciting the fluorophore (eq. 4), which is the electron acceptor in the cases under discussion, is represented by $E_{0,0}$. The electrostatic potential energy between the radical cation and anion is expressed using the Coulomb Law (eq. 5), where d is the center-to-center distance between the electron donor and the acceptor, and ε is the dielectric constant of the solvent. The E_{ox} and $-E_{red}$ terms are the cost of PeT, while the other two terms are the gain of energy.

Based on the analysis of the Rehm-Weller equation, high energy, short wavelength fluorophores have large values of $E_{0,0}$, therefore contribute favorably to PeT, and in another word, are relatively easy to be quenched. When the fluorophore is changed from 7-methoxycoumarin to 7-(*N*,*N*-diethylamino)coumarin, the absolute value of E_{red} increases while that of $E_{0,0}$ decreases, which collectively reduces the driving force of PeT. Assuming the

View Article Online
DOI: 10.1039/C7OB02235B

distance between donor and acceptor does not change upon the exchange of fluorophore, in order to maintain the thermodynamic driving force of PeT, the E_{ox} term of the e-donor has to decrease to offset the unfavorable changes of E_{red} and $E_{0,0}$. That means the e-donor must change accordingly to an electron-richer one.

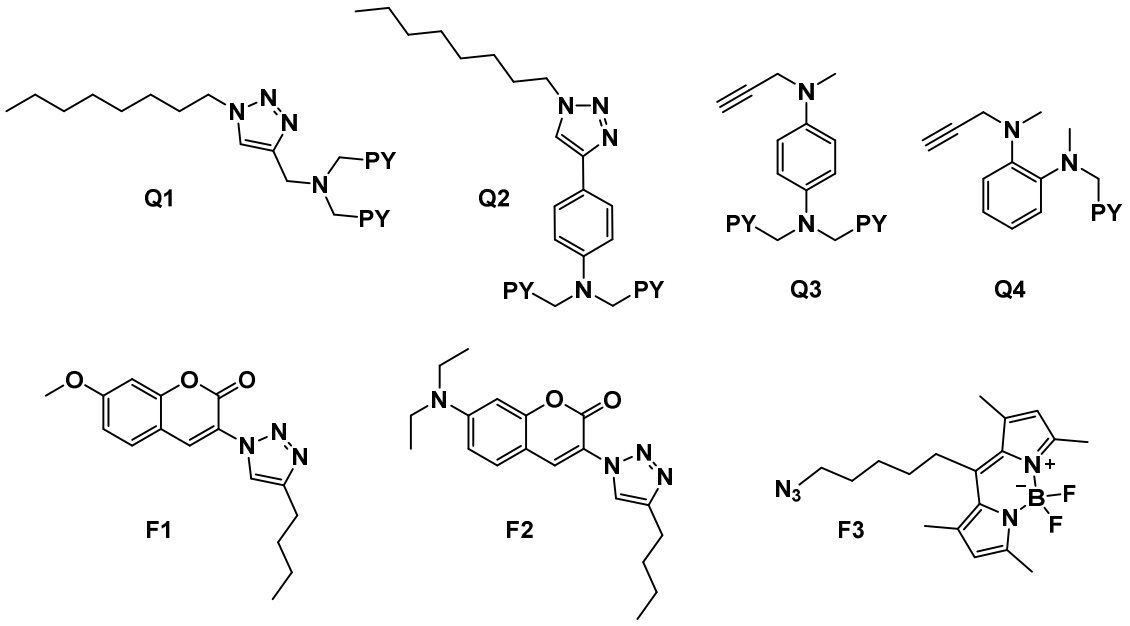

Fig. 4 Electron donors **Q1**-**Q4**, and fluorophores **F1**-**F3**.

The combination of four electron-donating ligands (**Q1**-**Q4** in Fig. 4) and three electron accepting fluorophores (**F1**-**F3** in Fig. 4) were studied using cyclic voltammetry to assess their effectiveness to act as components in zinc-switchable PeT systems. **Q1** is a tertiary amine, while **Q2**-**Q4** are anilino electron donors that incorporate zinc-coordinating pyridyl and/or triazolyl groups. Compounds **F1** and **F2** are differently substituted coumarin fluorophores, while **F3** is a BODIPY fluorophore. The E_{ox} of the electron donors **Q1**-**Q4** and the E_{red} of dyes **F1**-**F3** were

View Article Online
DOI: 10.1039/C7OB02235B

determined via cyclic voltammetry in acetonitrile. The ΔG°_{PeT} values of arbitrary quencher and fluorophore pairs were estimated using the Rehm-Weller equation,[39] and are listed in Table 1. In the calculations, the electrostatic term was omitted considering the large relative permittivity of the solvent under consideration – 37.5 of acetonitrile.

The oxidation and reduction potential values referenced to ferrocene are listed in Table 1. The tertiary amino electron donor **Q1** has an oxidation potential of 0.70 V. The first oxidation of the anilino-based **Q2** was found at 0.41 V. The first oxidation potential of *para*-diaminobenzene-based **Q3** dropped to -0.04 V, while the *ortho*-diaminobenzene-derived **Q4** was oxidized at 0.30 V. **Q3**, therefore, stood out as the most effective electron-donating quencher.

The reduction potential of 7-(*N*,*N*-diethyl)aminocoumarin (**F2** in Fig. 4) is larger than that of the 7-methoxycoumarin **F1** (Table 1), while the $E_{0,0}$ of **F2** is smaller than that of **F1**. Neither term favors **F2** in engaging PeT with **Q1**. The ΔG°_{PeT} value between **Q1** and **F2** is consequently positive (Table 1). For **F3**, although it has a small $E_{0,0}$, its reduction potential is also the lowest – i.e., the best electron acceptor. The collective effect of $E_{0,0}$ and E_{red} gives a favorable ΔG°_{PeT} when pairing with the tertiary amino quencher **Q1**. Not coincidentally, the combination of **F3** and DPA was used as a PeT-based zinc sensor.[40] Based on the calculated ΔG°_{PeT} values (Table 1), molecules equipped with an anilino-containing ionophore and any of the three fluorophores in Fig. 4 possess favorable ΔG°_{PeT} values needed to create a zinc-actuated PeT switch.

Table 1 Summary of cyclic voltammetry data and calculated ΔG°_{PeT} values (in red).

ΔG°_{PeT} (eV)	$\lvert E_{red} \rvert$ (V)[a]	$E_{0,0}$ (eV)	**Q1**	**Q2**	**Q3**	**Q4**
E_{ox} (V)[a]	-	-	0.70	0.41	-0.04	0.30
F1	1.88	3.26	-0.68	-0.97	-1.42	-1.08

View Article Online
DOI: 10.1039/C7OB02235B

F2	2.05	2.74	+0.01	-0.28	-0.73	-0.39
F3	1.69	2.49	-0.10	-0.39	-0.84	-0.50

a. Oxidation and reduction potentials are referenced to ferrocene in acetonitrile. The electrolyte is tetrabutylammonium perchlorate.

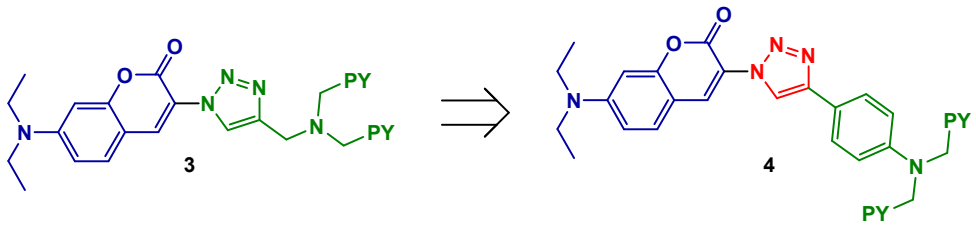

Fig. 5 Changing the ionophore of compound **3** from **Q1** to **Q2** to afford compound **4**.

3. The effect of anilino electron donor on the fluorescence and zinc-response of compound **4**.

Based on the data in Table 1, a fluorescent sensor that combines an anilino-DPA ionophore such as the one in **Q2** with fluorophore **F2** shall function as a PeT-based zinc sensor (compound **4** in Fig. 5). The absorption of 7-(*N*,*N*-diethylamino)coumarin corresponds nicely with the 405-nm laser that is equipped with our laser scanning confocal fluorescence microscope. The synthesis of compound **4** is depicted in Scheme S1. The fluorescence intensity of **4** increases upon titration of $Zn(ClO_4)_2$ in acetonitrile (Fig. 6). The fluorescence quantum yield of **4** increases by 90-fold upon the formation of the zinc complex, suggesting that the PeT process is switched 'off' after zinc binding.[41]

View Article Online
DOI: 10.1039/C7OB02235B

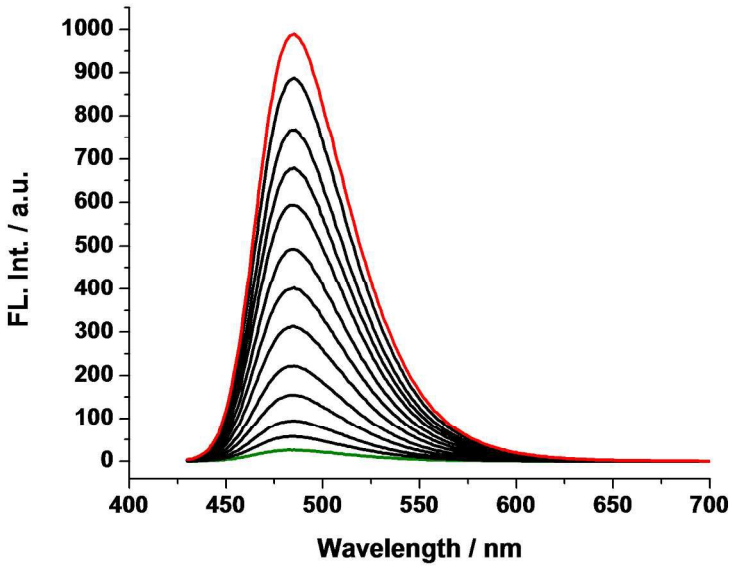

Fig. 6 Fluorescence spectra of compound **4** (9.5 μM, λ_{ex} = 420 nm) in the presence of $Zn(ClO_4)_2$ (0 – 14 μM) in acetonitrile. The initial and final spectra are coded green and red, respectively.

Compound **4** is excitable by visible light, which is an improvement over compound **2** that is excited in the UV region. The fluorescence sensitivity of compound **4** to the presence of zinc is restored from that of compound **3** by changing the PeT quencher, which is also the zinc ligand, from aliphatic DPA to anilino-DPA. These are the positive attributes of compound **4** with regard to the potential as a zinc sensor. The affinity of compound **4** to zinc,[42] however, likely is similar to that of **Newport Green PDX** ($K_{d(ZnL)}$ = 40 μM, Fig. 2), which is more than a thousand folds lower than that of the parent compound **2** ($K_{d(ZnL)}$ = 5.5 nM), the starting point of our improvement effort. In the next step, we aimed for increasing the zinc affinity while preserving the fluorescence sensitivity to zinc of **4** via structural modification of the quencher/ionophore component.

View Article Online
DOI: 10.1039/C7OB02235B

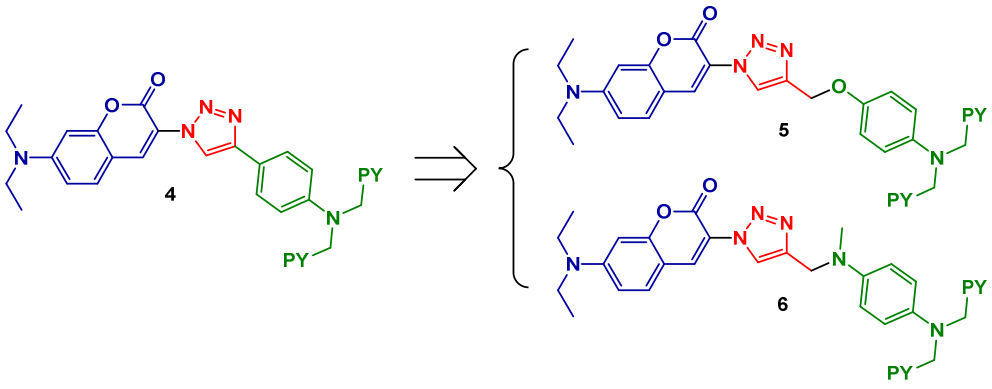

Fig. 7 Increasing the electron density of the anilino-containing quencher/ionophore in **4** to afford compounds **5** and **6**.

4. Increasing the electron density on the anilino ionophore. In compounds **5** and **6** (Fig. 7), alkoxy and *N*-methylamino groups are included at the *para* position of the anilino-DPA ionophore, respectively. This modification was aimed to increase the zinc affinity of the tridentate anilino-DPA ligand, while also easing the synthesis of the dialkylated aniline by increasing the nucleophilicity of the anilino moiety. The synthesis of compound **6** started with nucleophilic aromatic substitution between 1-fluoro-4-nitrobenzene and *N*-methylpropargylamine to afford compound **7** (Fig. 8). The nitro group was reduced by stannous chloride to afford **8**. Dialkylation of the anilino group of **8** was completed in an overnight reaction either with 2-pyridinecarboxaldehyde (reductive amination), or with 2-picolylbromide (S_N2 alkylation), rather than over multiple days as reported in other syntheses of anilino-DPA moieties.[33, 34] The faster anilino-DPA synthesis results from having the additional electron-donating amino group, which enhances the nucleophilicity of the unsubstituted amino group. Finally, copper(I)-catalyzed cycloaddition between azide **10**[43] and alkyne **9** afforded compound **6**.

View Article Online
DOI: 10.1039/C7OB02235B

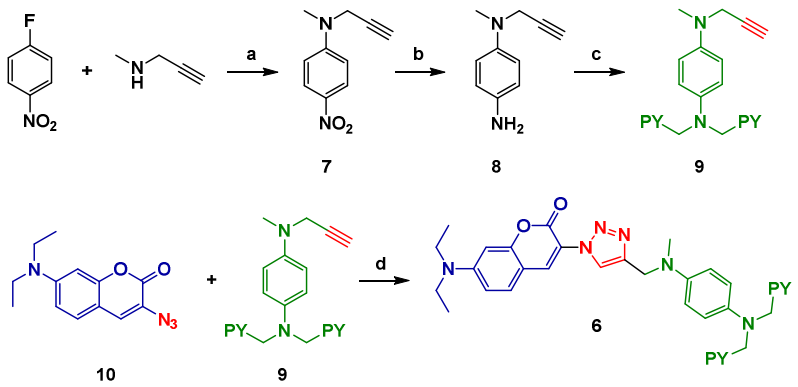

Fig. 8 Synthesis of compound **6**. Reagents and conditions: a) neat, *N*-methylpropargylamine (2 molar equiv.), rt, > 95%, or *N*-methylpropargylamine (1 molar equiv.), K_2CO_3, DMSO, 50 °C, overnight, 72%; b) $SnCl_2$, HCl (37%, v:v), overnight, 70%; c) 2-pyridinecarboxaldehyde, $NaBH(OAc)_3$, 1,2-dichloroethane, rt, 75%, or 2-picolylbromide hydrobromide, Na_2CO_3, EtOH, reflux, overnight, 46%; d) CuCl (20 mol%), THF, under argon, overnight, 60%.

The fluorescence quantum yield of compound **6** grew by 4.5-fold upon the formation of a zinc complex in acetonitrile (Fig. 9a). Fluorescence enhancement of compound **6** was also observed in a zinc titration experiment conducted in an aqueous buffer at pH 7.4 (Fig. 9b). Fitting the binding isotherm with a 1:1 stoichiometry yields a dissociation constant (K_d) of ZnL of 3 μM (Fig. 9c).[44] This value is more than 10-fold lower than that of **Newport Green PDX** ($K_{d(ZnL)}$ = 40 μM, Fig. 2), suggesting that *para*-*N*-methylamino group installed on the anilino-DPA ligand increases its affinity to zinc to the extent of an aliphatic DPA ligand as seen in compound **1** (K_d = 5 μM, Fig. 1). The fluorescence of compound **6** selectively responds to the presence of zinc over alkali and alkaline earth metal ions, as well as a few selected first-row transition metal ions (Fig. S3). Cadmium, however, elicits a similar emission enhancement from compound **6**. Compound **5**

View Article Online
DOI: 10.1039/C7OB02235B

(synthesis see Scheme S2) was also characterized, and up to 6-fold fluorescence enhancement upon zinc coordination in acetonitrile was observed (Table 2). Due to the similar aggregation issues under aqueous conditions to that we experienced with compound **4**,[42] the $K_{d(ZnL)}$ of compound **5** under pH neutral aqueous conditions was not determined.

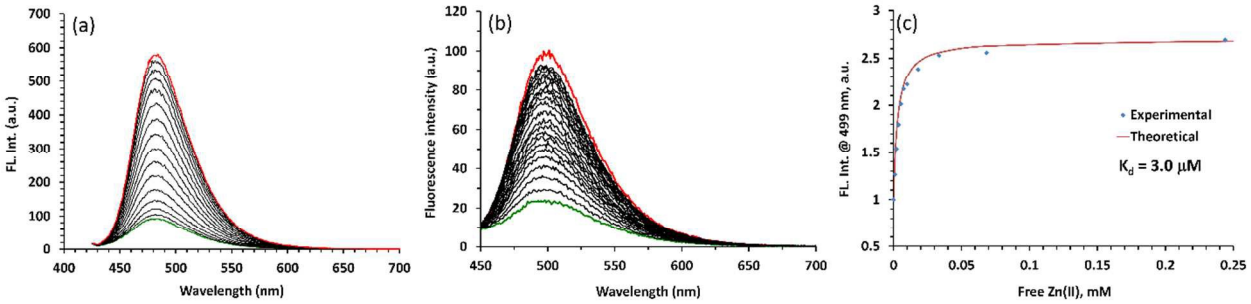

Fig. 9 Fluorescence spectra of (a) **6** (5 μM, λ_{ex} = 400 nm) in the presence of $Zn(ClO_4)_2$ (0-8.3 μM) in acetonitrile, and (b) **6** (6 μM, λ_{ex} = 410 nm) in the presence of $Zn(ClO_4)_2$ (0-7.3 mM) in an aqueous solution: [HEPES] = 100 mM, [citrate] = 10.0 mM, [KNO_3] = 100 mM, pH = 7.4. The initial and final spectra of each titration experiment are coded green and red, respectively. (c) Fluorescence intensity at 500 nm measured under conditions in (b) was fit as a function of 'free' zinc concentration, using a 1:1 binding model,[45] to yield a K_d value of 3 μM.

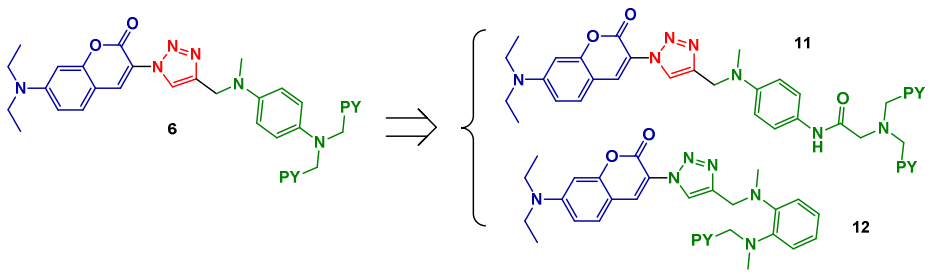

Fig. 10 Changing the zinc ligand portion of **6** to afford **11** and **12**.

View Article Online
DOI: 10.1039/C7OB02235B

5. Further increasing zinc affinity based on the structure of **6**. The effort of structural modification acted upon compound **6** was directed at increasing the zinc affinity further to a $K_{d(ZnL)}$ within or close to single nanomolars. Starting from compound **6**, two strategies were considered: the tridentate di(2-picolyl)amino (DPA) group in **6** could be replaced by a tetradentate ligand with an additional amide carbonyl arm[46, 47] to afford compound **11** (Fig. 10). In the second strategy, the DPA group on anilino could be moved to the *ortho* position in regard to the other amino group to potentially engage it, and the triazolyl group,[35] in binding zinc. Yet after numerous unsuccessful attempts of incorporating a DPA moiety *ortho* to an amino group, we resorted to synthesize compound **12** (Fig. 10), which has an *N*-methyl-*N*-2-picolylamino (MPA) group as the zinc binding ligand. The syntheses of **11** and **12** are depicted in Schemes S3-4.

Compound **11** exhibited up to 6.4-fold fluorescence enhancement in the presence of zinc perchlorate in acetonitrile (Fig. 11a). It has been reported that the instalment of an amide scaffold one methylene away from a DPA moiety results in a tetradentate ligand with zinc affinity in the nanomolar range.[48] The K_d of the zinc complex of compound **11** determined at pH 7.4 was 30 nM (Fig. 11c/d), which is in agreement with other zinc sensors containing the amide-DPA scaffold.[49, 50] This value is 100-fold higher than the zinc affinity of compound **6** and thus validating the strategy outlined earlier. The metal ion response profile of the emission of compound **11** is similar to that of compound **6** (Fig. S4). Compound **11** had the same λ_{em} for both zinc-free and zinc(II)-bound states as that of compound **6**. In the case of **12** (MPA as the zinc-binding unit, Fig. 11b), there was a 12-nm red-shift from the emission of the free ligand (λ_{em} = 482 nm) to that of the zinc complex (λ_{em} = 494 nm). The emission of compound **12** increased by

View Article Online
DOI: 10.1039/C7OB02235B

4.3-fold upon zinc complex formation in acetonitrile. The K_d of compound **12** under aqueous conditions was not determined due to the aggregation issues.[42]

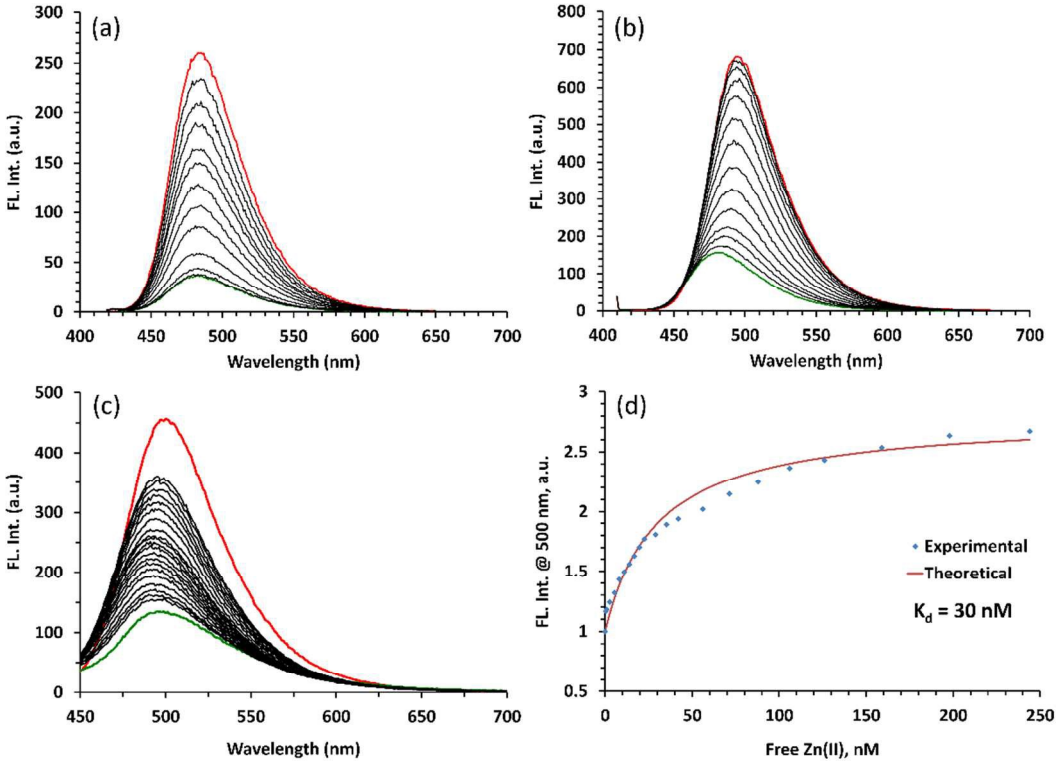

Fig. 11 Fluorescence spectra of (a) **11** (5 μM, λ_{ex} = 400 nm) in the presence of $Zn(ClO_4)_2$ (0-25 μM), (b) **12** (5 μM, λ_{ex} = 405 nm) in the presence of $Zn(ClO_4)_2$ (0-57 μM) in acetonitrile, and (c) **11** (6 μM, λ_{ex} = 410 nm) in the presence of $Zn(ClO_4)_2$ (0-7.9 mM) in an aqueous solution: [HEPES] = 100 mM, [ADA] = 10.0 mM, [KNO_3] = 100 mM, pH = 7.4. The initial and final spectra are coded green and red, respectively. (d) Fluorescence intensity at 500 nm of **11** was fit as a function of free zinc concentration, using a 1:1 binding model,[45] to yield a K_d value of 30 nM.

Table 2 Summary of photophysical properties of **4-6**, and **11-13** in acetonitrile.

View Article Online
DOI: 10.1039/C7OB02235B

Compound	λ_{abs} (nm)	λ_{em} (nm)	ϕ_L	ϕ_{ZnL}
4	413	486	0.005	0.45
5	385	484	0.09	0.54
6	416	499	0.02	0.09
11	421	495	0.02	0.05
12	407	482	0.07	0.25
13a	515	523	0.01	0.02
13b	496	503	0.04	0.13
13c	494	501	0.06	0.19

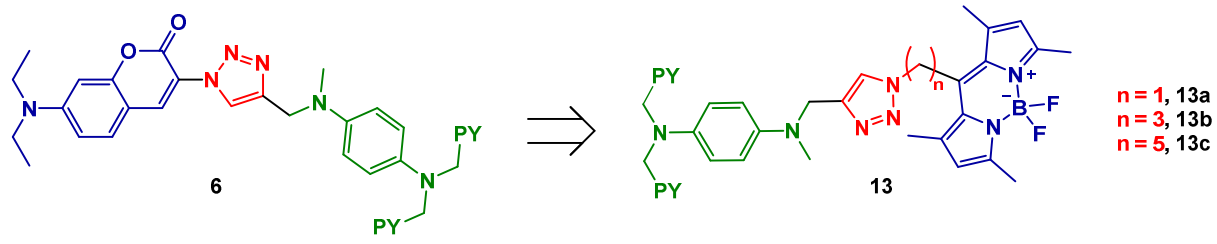

Fig. 12 Changing the fluorophore in **6** to afford compounds **13a-c**.

6. Effect on the PeT-switch by changing fluorophore, and distance between e-donor and e-acceptor. We were curious whether the *para*-amino-anilino-DPA quencher would work well with other fluorophores to afford zinc-actuated PeT switches. The BODIPY fluorophore was selected in this work because of its brightness and photostability in cell imaging.[51-54] This dye has been incorporated as a reporter in fluorescence sensors for zinc.[55, 56] The effectiveness of BODIPY and anilino group to act as a PeT switch has been demonstrated in one case.[57] Compounds **13a-c** (Fig. 12) were prepared (Scheme S5) that differ in the length of the alkyl linker connecting the

View Article Online
DOI: 10.1039/C7OB02235B

fluorophore to the triazolyl group. By comparing the properties of **13a-c**, the effect of the linker length on the performance of these compounds as zinc sensors was demonstrated.

View Article Online
DOI: 10.1039/C7OB02235B

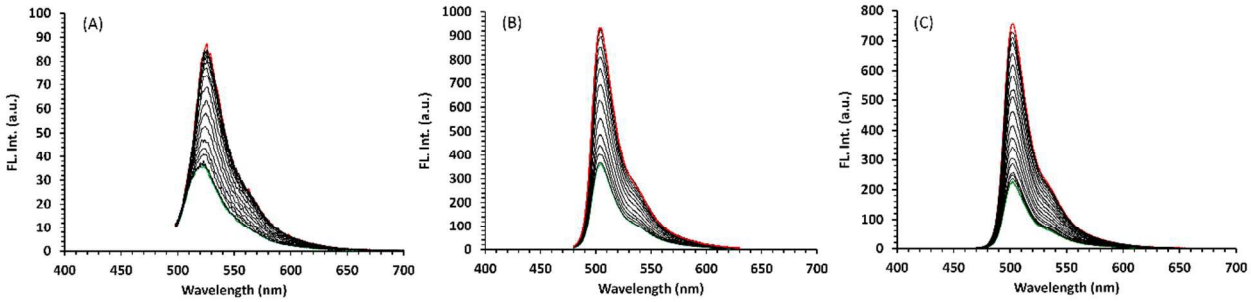

Fig. 13 Fluorescence spectra of **13a-c** (2 μM) in acetonitrile in the presence of $Zn(ClO_4)_2$ (0-30 μM). (A) **13a** (λ_{ex} = 488 nm), (B) **13b** (λ_{ex} = 465 nm), and (C) **13c** (λ_{ex} = 465 nm). The initial and final spectra of each titration experiment are coded green and red, respectively.

The zinc sensitivity of the fluorescence of compounds **13a-c** were studied (Fig. 13). In all zinc titration experiments, the addition of $Zn(ClO_4)_2$ led to an increase in fluorescence as expected from a zinc-actuated PeT switch. The photophysical data of **13a-c** are included in Table 2. Compound **13a** has the smallest fluorescence quantum yield values in both free and zinc-bound states. The smallest distance (one methylene) between the zinc-binding DPA unit and the fluorophore appears to result in a low quantum yield of the BODIPY fluorophore. Compounds **13b** and **13c** with longer linkers separating the fluorophore and the quencher have similarly higher quantum yield values.

7. Comments on the fluorescence quantum yields. In acetonitrile, zinc binding was able to restore the fluorescence quantum yields of compounds **4** and **5** to 0.45 and 0.54, respectively, while smaller extents of enhancement were observed for other compounds that contain the *para*-amino anilino quencher component (Table 2). The oxidation potential of zinc complex of **Q2**, which is the quencher component in compound **4**, was not measurable within the voltage cycling window in this study, suggesting that zinc complexation with **Q2** increased the oxidation

View Article Online
DOI: 10.1039/C7OB02235B

potential of **Q2** to a sufficiently high level so that the PeT process in compound **4** is effectively stopped. By comparison, the oxidation potential of compound **Q3** was increased from -0.04 V to 0.48 V in the presence of an equal molar amount of $Zn(ClO_4)_2$.[58] The effect of zinc binding on increasing the oxidation potential of this quencher is apparent, but not up to even the level of tertiary amino group in its free form (0.70 V). Therefore, the zinc complex of **Q3**, and by analogy the zinc complexes of the quencher components in compounds **6**, **11**, **12**, and **13a-c**, are still sufficiently electron-rich to keep the PeT channels open, which diminish the emission of the fluorophores they are attached to. Compound **12** has the highest quantum yield (0.25) in the zinc-bound form among these compounds. The ability to engage both amino groups in zinc binding might have hindered the PeT pathway more effectively in the zinc-bound form than the case of compound **6**.

8. Visualizing zinc ions in live HeLa cells. Fluorescent ligands **4-6** and **11-13** were evaluated for their potentials in visualizing zinc ions in live HeLa cells. All cells were incubated in a medium containing 1-4 micromolars of one of the dyes for 30 min. The medium was then replaced with fresh medium that contained either basal or enriched level of zinc ions in the form of $ZnCl_2$. The images were acquired by different experimenters at different time periods of this project. Therefore, the images taken using the same parameter sets are grouped together, so that within each group the images are comparable in emission intensity. The fluorescence microscopic images of cells stained with compounds **4-6** (λ_{ex} = 405 nm), compounds **11** and **12** (λ_{ex} = 405 nm), and compounds **13a-c** (λ_{ex} = 488 nm) are shown in Figures 14-16, respectively.

View Article Online
DOI: 10.1039/C7OB02235B

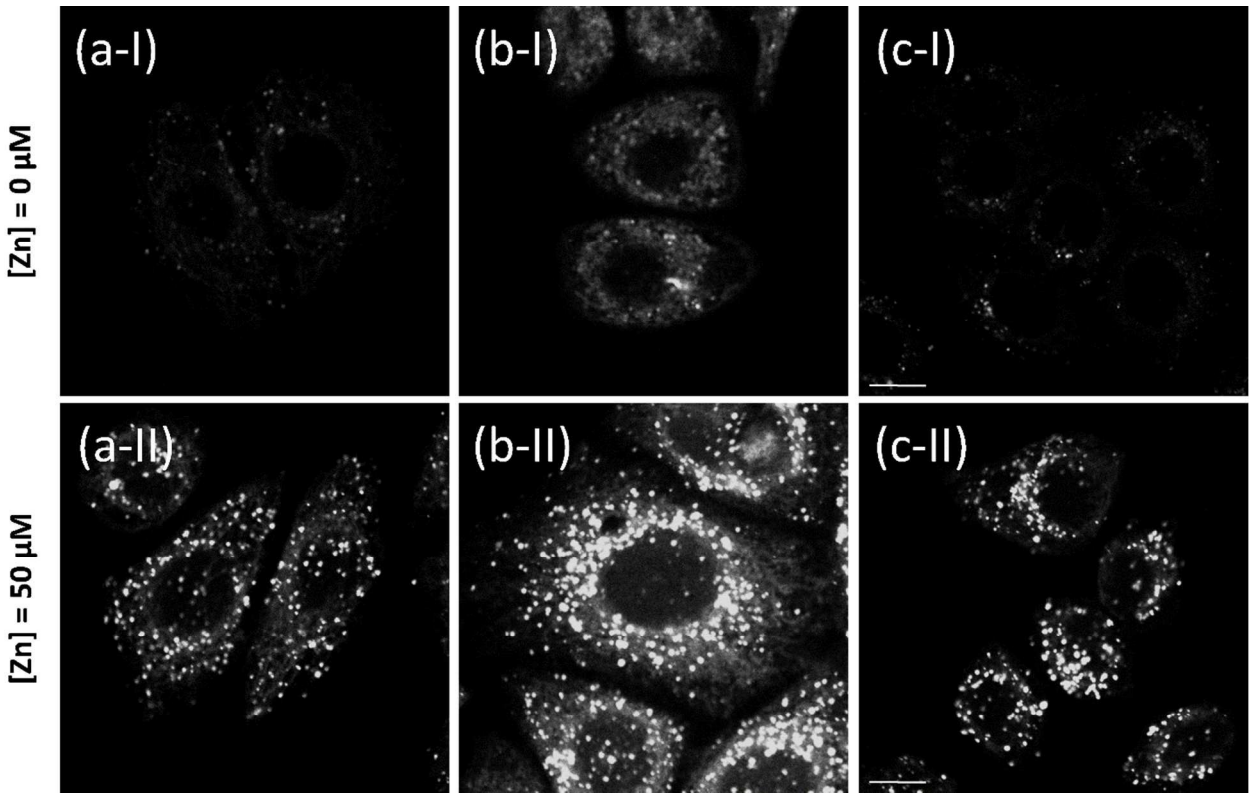

Fig. 14 Laser scanning confocal fluorescence microscopic images of compounds **4** (a), **5** (b), and **6** (c) in live HeLa (S3) cells. The incubating concentration was 2 μM each. Images in the top row were taken in the absence of supplemented $ZnCl_2$. Images in the bottom row were taken in the presence of 50 μM added $ZnCl_2$. [sodium pyrithione] = 50 μM; λ_{ex} = 405 nm; scale bar = 10 μm.

The images on the top row of Fig. 14 show cells that were loaded with compounds **4-6** (from a-c) in a media without supplemented zinc. The bottom images show the fluorescence responses from these compounds after the media was supplemented with 50 μM $ZnCl_2$. All the images were acquired using the same parameter set. Therefore, the observed intensity of these images is comparable. The images of cells labeled with **4** (Fig. 14a-I) and **6** (Fig. 14c-I) show least fluorescence intensity, likely due to the background fluorescence of the sensors in the unbound

View Article Online
DOI: 10.1039/C7OB02235B

state. The image associated with **5** (Fig. 14b-I) shows a larger fluorescence intensity; but there is still a large contrast between itself and the corresponding bottom image of cells (Fig. 14b-II) bathed in a media supplemented with zinc. Large fluorescence enhancement is also evident in the fluorescence images of cells with **4** (Fig. 14a-II) and **6** (Fig. 14c-II) in zinc-enriched media.

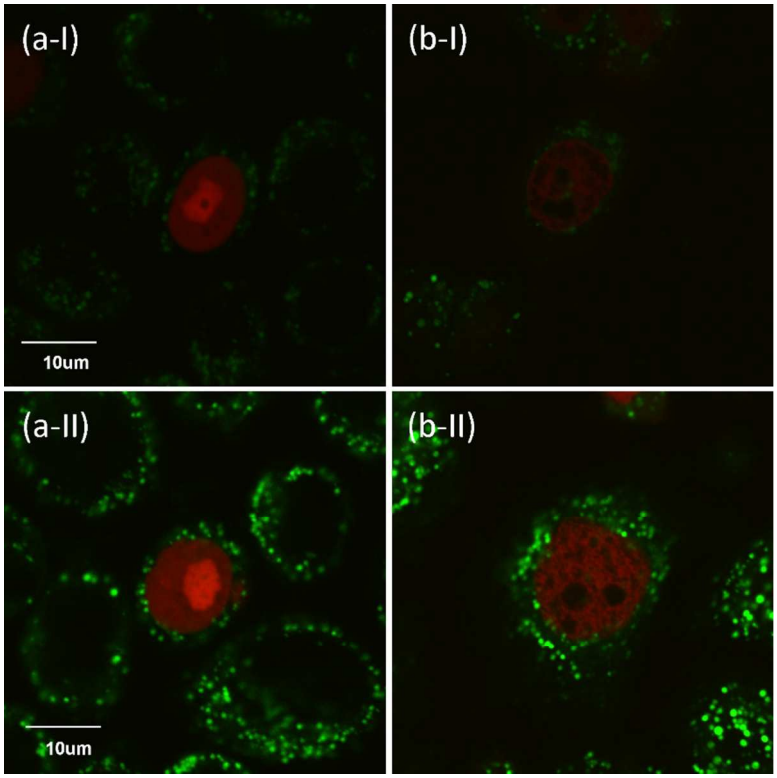

Fig. 15 Laser scanning confocal fluorescence microscopic images of compounds **11** (a, incubating concentration 1 μM) and **12** (b, 1 μM) in live HeLa (S3) cells. Images in the top row were taken in the absence of supplemented $ZnCl_2$. Images in the bottom row were taken in the presence of 50 μM added $ZnCl_2$. Green channel (λ_{ex} = 405 nm, emission window 460-560 nm), red channel (λ_{ex} = 488 nm, emission window 590-630 nm). [sodium pyrithione] = 50 μM.

View Article Online
DOI: 10.1039/C7OB02235B

Similar to compounds **4-6**, **11** and **12** showed the ability to reflect changes of intramolecular zinc concentrations in living HeLa (S3) cells, as the intensity of the bottom images is higher than that on the top row (Fig. 15). The incubating concentrations of the dyes was 1 μM each, despite the unremarkable fluorescence quantum yield values of these two compounds. These cells were transfected with mCherry-H2B-6,[59] a red fluorescent protein that marks nuclei of mammalian cells. The emission from mCherry-H2B-6 in the red channel was used as nuclear counter stain.

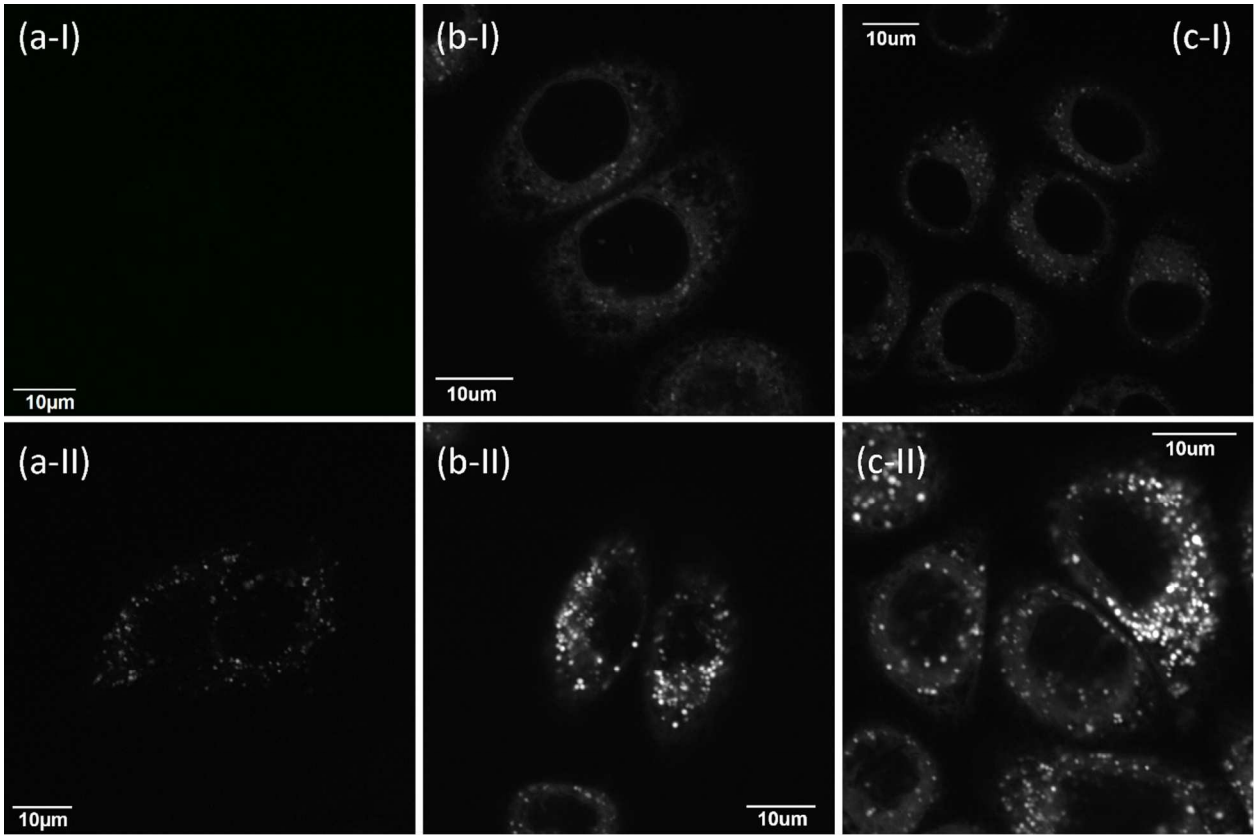

Fig. 16 Laser confocal fluorescence microscopic images of compounds **13a** (a), **13b** (b), and **13c** (c) in live HeLa (S3) cells. The incubating concentration was 4 μM each. Images in the top row were taken in the absence of supplemented $ZnCl_2$. Images in the bottom row were taken in the presence of 50 μM added $ZnCl_2$. [sodium pyrithione = 50 μM]; λ_{ex} = 488 nm; scale bar = 10 μm.

View Article Online
DOI: 10.1039/C7OB02235B

BODIPY-derived compounds **13a-c** were tested in live HeLa (S3) cells to see if the chain length affected the performance of the dyes in reporting intracellular zinc alterations. Fig. 16 shows the three compounds imaged in the cell under both basal (no added zinc) or zinc-supplemented (50 μM) conditions. Compounds **13b** and **13c** both show a larger contrast between zinc-free and supplemented incubation conditions than compound **13a**, which afforded overall dimmer emission than **13b** and **13c**. These imaging data are consistent with the difference in fluorescence quantum yields of the three compounds.

Conclusion

The initial attempt to generate visible light-excitable, PeT-based fluorescent indicators for zinc ions with an aliphatic amine quencher based on a UV-absorbing precursor was unsuccessful because a favorable thermodynamic driving force of electron transfer was lost. Cyclic voltammetry studies showed that anilino-based ionophores/quenchers would be effective in the zinc-actuated PeT-switch. Due to the difficulties associated with synthesizing anilino-DPA ligands, electron-donating groups were placed *para* to the anilino nitrogen to increase its nucleophilicity. The syntheses of the new compounds (**5** and **6**) were accomplished with less time, as a result of the additional electron-donating substituents on the anilino moiety. All the anilino-DPA-containing indicators undergo various degrees of fluorescence enhancement upon binding zinc, as anticipated from zinc-actuatable PeT switches. The installment of electron-donating groups onto the anilino moiety also increases the zinc affinity of the indicators. Using *para*-amino-anilino group as a quencher is effective in pairing up with both 7-*N*,*N*-diethylaminocoumarin and BODIPY fluorophores. Three BODIPY-derived compounds were made that differ in the linker length between the fluorophore and the quencher/ionophore. The

View Article Online
DOI: 10.1039/C7OB02235B

one with the shortest linker (**13a**) suffers with relatively low fluorescence quantum yields in both zinc-free and zinc-bound forms. All the anilino-DPA-containing sensors were evaluated for their potentials as zinc sensors in live cell imaging experiments, and except **13a** are all similarly capable of reporting the changes of intracellular zinc concentrations. These compounds can be excited at either 405 nm or 488 nm with various affinities to zinc. The strategy of using anilino-DPA as a key component of zinc receptor and electron transfer-based quencher appears to be applicable in producing zinc sensitive dyes with various excitation energy, emission colors, and effective concentration ranges.

ACKNOWLEDGMENT

This work was supported by the National Science Foundation (CHE1566011).

Electronic supplementary information (ESI) available: Synthetic procedures and characterizations of new compounds, procedures of spectroscopic data acquisition, cyclic voltammetry, cell culture and fluorescence microscopy, and copies of NMR spectra of new compounds.

Notes and References:

1. R. A. Colvin, A. I. Bush, I. Volitakis, C. P. Fontaine, D. Thomas, K. Kikuchi and W. R. Holmes, *American Journal of Physiology - Cell Physiology*, 2008, **294**, C726.
2. A. Krężel and W. Maret, *J. Biol. Inorg. Chem.* 2006, **11**, 1049-1062.
3. L. A. Gaither and D. J. Eide, *Biometals*, 2001, **14**, 251-270.
4. D. J. Eide, *Biochim. Biophys. Acta*, 2006, **1763**, 711-722.
5. T. K. Fukada, Taiho, *Zinc Signals in Cellular Functions and Disorder*, Springer, Tokyo, 2014.
6. R. A. Bozym, R. B. Thompson, A. K. Stoddard and C. A. Fierke, *ACS Chem. Biol.* 2006, **1**, 103-111.

View Article Online
DOI: 10.1039/C7OB02235B

7. Y. Qin, P. J. Dittmer, J. G. Park, K. B. Jansen and A. E. Palmer, *Proc. Nat. Acad. Sci.* 2011, **108**, 7351-7356.
8. S. L. Sensi, L. M. T. Canzoniero, S. P. Yu, H. S. Ying, J.-Y. Koh, G. A. Kerchner and D. W. Choi, *J. Neurosci.* 1997, **17**, 9554.
9. J. L. Vinkenborg, T. J. Nicolson, E. A. Bellomo, M. S. Koay, G. A. Rutter and M. Merkx, *Nat. Meth*. 2009, **6**, 737-740.
10. D. B. Murphy and M. W. Davidson, *Fundamentals of Light Microscopy and Electronic Imaging*, Wiley-Blackwell, Hoboken, NJ, Second edn., 2013.
11. R. P. Haugland, *The Molecular Probes® Handbook - A Guide to Fluorescent Probes and Labeling Technologies*, Invitrogen, 11th edn., 2010.
12. E. L. Que, D. W. Domaille and C. J. Chang, *Chem. Rev.*, 2008, **108**, 1517-1549.
13. Z. Xu, J. Yoon and D. R. Spring, *Chem. Soc. Rev.*, 2010, **39**, 1996-2006.
14. Z. Huang and S. J. Lippard, *Methods in Enzymology*, 2012, **505**, 445-468.
15. K. P. Carter, A. M. Young and A. E. Palmer, *Chem. Rev.*, 2014, **114**, 4564-4601.
16. Zhu, L.; Yuan, Z.; Sreenath, K.; Simmons, J. T., *RSC Adv.* 2014, **4**, 20398-20440.
17. (a) Y. Chen, Y. Bai, Z. Han, W. He and Z. Guo, *Chem. Soc. Rev.*, 2015, **44**, 4517-4546; (b) A. M. Hessels and M. Merkx, *Metallomics*, 2015, **7**, 258-266.
18. Y. Ding, Y. Tang, W. Zhu and Y. Xie, *Chem. Soc. Rev.*, 2015, **44**, 1101-1112.
19. A. P. de Silva, H. Q. N. Gunaratne, T. Gunnlaugsson, A. J. M. Huxley, C. P. McCoy, J. T. Rademacher and T. E. Rice, *Chem. Rev.*, 1997, **97**, 1515-1566.
20. B. Valeur and I. Leray, *Coord. Chem. Rev.*, 2000, **205**, 3-40.
21. A. P. de Silva, T. S. Moody and G. D. Wright, *Analyst*, 2009, **134**, 2385-2393.
22. B. Valeur, *Molecular Fluorescence Principles and Applications*, Wiley, Weinheim, 2010.
23. M. D. Pluth, E. Tomat and S. J. Lippard, *Ann. Rev. Biochem.*, 2011, **80**, 333-355.
24. S. A. de Silva, A. Zavaleta, D. E. Baron, O. Allam, E. V. Isidor, N. Kashimura and J. M. Percapio, *Tetrahedron Lett.*, 1997, **38**, 2237-2240.
25. G. K. Walkup, S. C. Burdette, S. J. Lippard and R. Y. Tsien, *J. Am. Chem. Soc.*, 2000, **122**, 5644-5645.
26. S. C. Burdette, G. K. Walkup, B. Spingler, R. Y. Tsien and S. J. Lippard, *J. Am. Chem. Soc.*, 2001, **123**, 7831-7841.
27. K. Komatsu, K. Kikuchi, H. Kojima, Y. Urano and T. Nagano, *J. Am. Chem. Soc.*, 2005, **127**, 10197-10204.
28. T. Hirano, K. Kikuchi, Y. Urano and T. Nagano, *J. Am. Chem. Soc.*, 2002, **124**, 6555-6562.
29. K. R. Gee, Z.-L. Zhou, D. Ton-That, S. Sensi and J. H. Weiss, *Cell Calcium*, 2002, **31**, 245-251.
30. See the work on the impact of the electronic structure of phenyl moiety on the PeT efficiency to the xanthene fluorophore the structural framework of fluorescein (#30 and #31): T. Ueno, Y. Urano, K.-i. Setsukinai, H. Takakusa, H. Kojima, K. Kikuchi, K. Ohkubo, S. Fukuzumi and T. Nagano, *J. Am. Chem. Soc.*, 2004, **126**, 14079-14085.
31. Y. Urano, M. Kamiya, K. Kanda, T. Ueno, K. Hirose and T. Nagano, *J. Am. Chem. Soc.*, 2005, **127**, 4888-4894.
32. P. Ashokkumar, V. T. Ramakrishnan and P. Ramamurthy, *J. Phys. Chem. A*, 2011, **115**, 14292-14299.
33. S. C. Burdette and S. J. Lippard, *Inorg. Chem.*, 2002, **41**, 6816-6823.

View Article Online
DOI: 10.1039/C7OB02235B

34. Z. Jiang, R. Deng, L. Tang and P. Lu, *Sensors and Actuators B: Chemical*, 2008, **135**, 128-132.
35. S. Huang, R. J. Clark and L. Zhu, *Org. Lett.*, 2007, **9**, 4999-5002.
36. H. A. Michaels, C. S. Murphy, R. J. Clark, M. W. Davidson and L. Zhu, *Inorg. Chem.*, 2010, **49**, 4278-4287.
37. J. T. Simmons, J. R. Allen, D. R. Morris, R. J. Clark, C. W. Levenson, M. W. Davidson and L. Zhu, *Inorg. Chem.*, 2013, **52**, 5838-5850.
38. Y. Zhou, K. Liu, J.-Y. Li, Y. Fang, T.-C. Zhao and C. Yao, *Org. Lett.*, 2011, **13**, 1290-1293.
39. D. Rehm and A. Weller, *Isr. J. Chem.*, 1970, **8**, 259-271.
40. Y. Wu, X. Peng, B. Guo, J. Fan, Z. Zhang, J. Wang, A. Cui and Y. Gao, *Org. Biomol. Chem.*, 2005, **3**, 1387-1392.
41. Zinc-dependent fluorescence enhancement of **4** and other compounds reported in this work was also observed in aqueous based buffers. However, the attempts to determine the zinc affinities values with meaningful precision and reproducibility of some of these compounds in aqueous based buffers at various pH values were not successful, due to the aggregation of either the free ligand or the zinc-bound form in all the buffers that we routinely used for this type of characterizations in the pH range of 4.5-7.4.
42. The zinc affinity of compound **4** should be comparable to that of **Newport Green PDX**, K_d = 40 μM, because both share the same anilino-DPA ligand for zinc.
43. K. Sivakumar, F. Xie, B. M. Cash, S. Long, H. N. Barnhill and Q. Wang, *Org. Lett.*, 2004, **6**, 4603-4606.
44. Titration data collected within the zinc buffering range of citrate were used in the fitting, which accounts for 70% of the overall fluorescence enhancement. There was further fluorescence intensity growth (the rest 30%) after zinc concentration exceeded the buffering range of citrate. We speculate that the change at high zinc concentrations, which was not used in the fitting of K_d, is attributed to the zinc coordination at the triazolyl/anilino bidentate site, *para* to the anilino-DPA position.
45. G. Grynkiewicz, M. Poenie and R. Y. Tsien, *J. Biol. Chem.*, 1985, **260**, 3440-3450.
46. Z. Xu, K.-H. Baek, H. N. Kim, J. Cui, X. Qian, D. R. Spring, I. Shin and J. Yoon, *J. Am. Chem. Soc.*, 2010, **132**, 601-610.
47. S. Sumiya, Y. Shiraishi and T. Hirai, *J. Phys. Chem. A*, 2013, **117**, 1474-1482.
48. Z. Xu, X. Liu, J. Pan and D. R. Spring, *Chem. Commun.*, 2012, **48**, 4764-4766.
49. Y. Cai, X. Meng, S. Wang, M. Zhu, Z. Pan and Q. Guo, *Tetrahedron Lett.*, 2013, **54**, 1125-1128.
50. O. A. H. Åstrand, L. P. E. Austdal, R. E. Paulsen, T. V. Hansen and P. Rongved, *Tetrahedron*, 2013, **69**, 8645-8654.
51. T. Kowada, H. Maeda and K. Kikuchi, *Chem. Soc. Rev.*, 2015, **44**, 4953-4972.
52. A. Loudet and K. Burgess, *Chem. Rev.*, 2007, **107**, 4891-4932.
53. J.-S. Lee, N.-y. Kang, Y. K. Kim, A. Samanta, S. Feng, H. K. Kim, M. Vendrell, J. H. Park and Y.-T. Chang, *J. Am. Chem. Soc.*, 2009, **131**, 10077-10082.
54. N. Boens, V. Leen and W. Dehaen, *Chem. Soc. Rev.*, 2012, **41**, 1130-1172.
55. W. Qin, W. Dou, V. Leen, W. Dehaen, M. Van der Auweraer and N. Boens, *RSC Adv.*, 2016, **6**, 7806-7816, and references therein.
56. J. Cao, C. Zhao, X. Wang, Y. Zhang and W. Zhu, *Chem. Commun.*, 2012, **48**, 9897-9899.

View Article Online
DOI: 10.1039/C7OB02235B

57. H. Koutaka, J.-i. Kosuge, N. Fukasaku, T. Hirano, K. Kikuchi, Y. Urano, H. Kojima and T. Nagano, *Chem. Pharm. Bull.*, 2004, **52**, 700-703.
58. See another electrochemical study on the effect of metal coordination on the oxidation potential of the ligand: R. Sahli, N. Raouafi, K. Boujlel, E. Maisonhaute, B. Schollhorn and C. Amatore, *New J. Chem.*, 2011, **35**, 709-715.
59. M. A. Kuipers, T. J. Stasevich, T. Sasaki, K. A. Wilson, K. L. Hazelwood, J. G. McNally, M. W. Davidson and D. M. Gilbert, *J. Cell Biol.*, 2011, **192**, 29-41.

View Article Online
DOI: 10.1039/C7OB02235B

Graphical Abstract

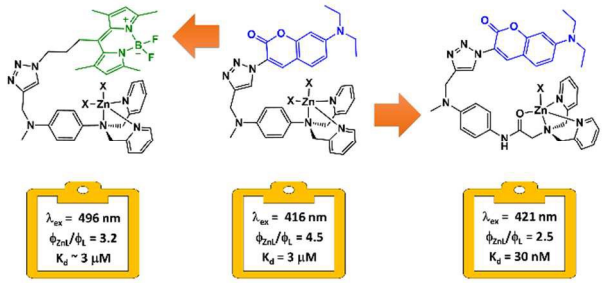

View Article Online
DOI: 10.1039/C7OB02235B

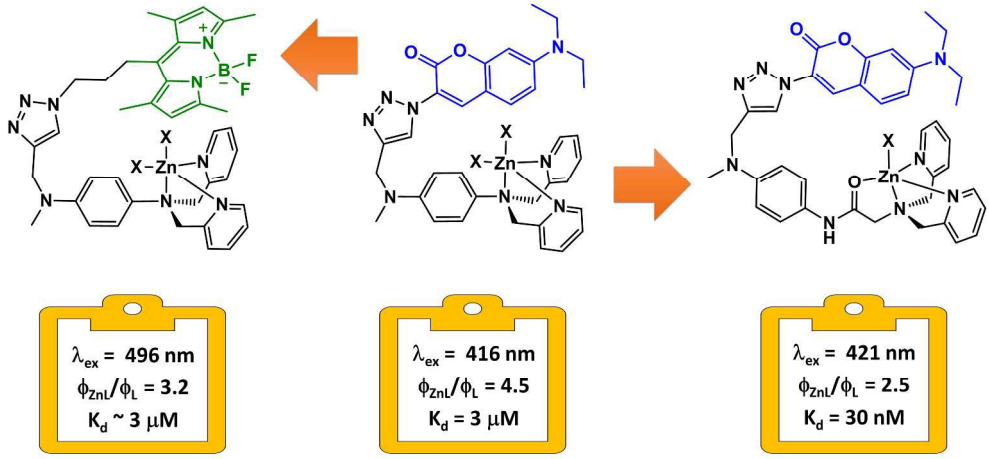

914x457mm (96 x 96 DPI)